Quantum pressure and chemical bonding: Influence of magnetic fields on electron localization

Jianmin Tao, Shi Liu, Fan Zheng, and Andrew M. Rappe

Phys. Rev. B **92**, 060401 — Published 3 August 2015

DOI: 10.1103/PhysRevB.92.060401

Quantum pressure and chemical bonding: Influence of magnetic fields on electron localization

Jianmin Tao,* Shi Liu, Fan Zheng, and Andrew M. Rappe
Department of Chemistry, University of Pennsylvania, Philadelphia, PA 19104-6323, USA
(Dated: June 4, 2015)

Chemical bonding is the central concept of chemistry that has been used to explain the properties of molecules and solids as well as chemical processes. In recent years, considerable progress has been made toward a simple and yet fundamental understanding of this concept for isolated systems. Here we propose the quantum pressure to study electron localization in molecules and solids as well as the influence of an external magnetic field. A high pressure indicates chemical bonding and electron localization, while a low pressure indicates intershell region and electron delocalization. We find that electrons become more localized between nuclei when exposed to a magnetic field. We demonstrate that our quantum pressure not only can reveal electronic shell structure of atoms, but also can be used to visualize chemical bonding in molecules and solids, significantly extending the applicability of this tool to wide-ranging problems.

PACS numbers: 31.10.+z, 71.15.-m, 75.10.-b

Since the concept of the chemical bond was originally introduced one century ago [1], it has undergone a series of evolutions [2], leading to modern chemical bond theory of two schemes: valence bond theory and molecular orbital theory, both of which stem from the Pauli exclusion principle and involve the linear combination of atomic orbitals (LCAO) [3, 4]. A subset of descriptive concepts derived from the chemical bond theory, such as atomic shell structure, electron-pair bond, lone electron pair, conjugated π-subsystem, bond order, etc. have become the standard language of chemistry. According to the valence bond theory, electrons become localized in pairs between nuclei when a molecule is formed. The nature of the chemical bond can be rigorously understood by quantum-mechanical laws such as wave function-based *ab initio* methods and first-principles approach (e.g., density functional theory [5]). However, there is no procedure that can extract an intuitive picture of the chemical bond from numerical data, because either the wave function or the electron density alone cannot clearly reveal the bonding structure. Chemists tend to rely on the concepts that are less rigorous but can be easily explained. Theories based on descriptive concepts such as VSEPR (valence shell electron pair repulsion theory) [6, 7] and orbital hybridization [3, 4] are still popular today. However, it is a great challenge to develop the breadth of the concept and make it as rigorous as we can, yet as simple as possible, so that it is more powerful and more useful.

Orbital overlap population analysis [8] based on the Pauli exclusion principle provides an elegant way to understand the chemical bond in terms of atomic orbital contributions. The idea is that one can express the wave functions in terms of the LCAO, whose coefficients can be calculated with the variational approach. From the LCAO coefficients, we can easily identify the contribution of each atomic orbital to the chemical bond, including bonding, non-bonding, and anti-bonding. Since the analysis can be easily understood, it has been widely used to describe the chemical bonding structure of π-subsystems. Based on this method, Dronskowski and Blöchl [9] proposed crystal orbital Hamilton populations (COHP) to study electron localization in solids. COHP offers an alternative way to visualize the chemical bond from energy resolution via population weighted density of states.

A frequently-asked question is "What does a chemical bond look like?". To explore the answer, Bader [10] proposed an electron localization indicator based on the Laplacian of the density $\nabla^2 n(\mathbf{r})$, which can reveal the bonding structures intuitively. This leads to the theory of atoms in molecules [10], offering a rigorous interpretation of the descriptive concept "atoms in molecules" [4]. It has been applied to study the electron localization in solids [11]. However, $\nabla^2 n(\mathbf{r})$ is a mathematical construction. In the search for electron localization indicators, an important step was made by Becke and Edgecombe [12]. They constructed an electron localization indicator, called electron localization function (ELF), from the curvature of the conditional pair probability. It was shown [13] that the ELF can reveal excellent bonding structures. In addition, it can be interpreted in terms of the Pauli exclusion principle and is uniquely defined without any ambiguity [14]. Due to its simplicity and the remarkable properties, it has been widely used to study the bonding structures of molecules and solids [15, 16]. In particular, it was extended [17] to time-dependent situations to visualize bond breaking and formation.

In iso-orbital regions of atoms and molecules such as the core region, pair bond region, and the density tail, the non-interacting kinetic energy density $\tau(\mathbf{r}) = (1/2)\sum_l |\nabla\phi_l(\mathbf{r})|^2$ tends to the von Weizäscker kinetic energy density $\tau^W(\mathbf{r}) = |\nabla^2 n|/8n^2$, while in other regions such as intershell regions, $\tau^W < \tau$. In the uniform electron gas, $\tau(\mathbf{r})$ reduces to the Thomas-Fermi kinetic energy density, while $\tau^W(\mathbf{r})$ vanishes. Therefore, the ra-

tio τ^W/τ can be used to reveal the bonding structure. Because of this feature, this combination [18] has been employed to construct density functional approximations. Recently, de Silva and Corminboeuf [19] suggested a density-based bonding descriptor, which can clearly exhibit both covalent and non-covalent bonding.

The ELF (and other bonding indicators) have achieved practical success in the description of the chemical bond. When a molecule is exposed to an external field, the electron density will be deformed in response to the external field. The ELF can still capture part of this effect by the implicit dependence of orbitals and the electron density on the external field. This effect may be properly described by the quantum pressure $p(\mathbf{r})$ [20–22], a physically meaningful quantity related to the Hamiltonian [23, 24]. It was shown [22] that, like the ELF, $p(\mathbf{r})$ can excellently reveal atomic shell structure. Since $p(\mathbf{r})$ describes the local stress or force on electrons, it should be able to reveal the bonding structure of molecules as well. However, our study shows that the original formulation of $p(\mathbf{r})$ does not clearly display the chemical bonding (see Fig. S1 in Supplemental Material). We identify that this problem is simply due to the $\nabla^2 n(\mathbf{r})$ term [Eq. (2) below]. Recent works have shown [25–28] that this difficulty can be reduced or fixed by the adjustment of the amount of $\nabla^2 n(\mathbf{r})$ in the kinetic part of the stress tensor, making use of the fact that there is an ambiguity in the definition of the kinetic energy density and the stress tensor. Since this offers flexibilities in optimizing the bonding index, without violation of any exact condition, a growing body of research regarding this ambiguity is accumulating in recent years.

Study of the influence of external magnetic fields on molecules and solids has long been a topic of interest. Many current-density functional theory (CDFT) methods [29, 30] have been proposed to describe this effect. In recent years, many papers have appeared studying magnetic field effects on chemical reactions [31, 32]. Based on experimental observations, controversial views on the influence of magnetic fields was recently proposed [33]. To have an intuitive and yet fundamental understanding of this effect on the chemical bonding, here we formulate the quantum pressure in a magnetic field based on the stress tensor. Then we generalize it to finite systems to study the bonding structure of molecules and solids, with and without magnetic fields. We find that the quantum pressure can clearly exhibit the chemical bonding, and that electrons in a molecule become slightly more localized between nuclei, when exposed to a magnetic field.

The quantum pressure is defined as one-third of the trace of the stress tensor in quantum systems. It describes the local force density exerted on electrons. However, in addition to the Laplacian discussed above, it can be also altered by adding any divergence-free stress tensor without changing the force [34, 35]. To make clarification, we start with the conventional definition of the stress tensor satisfying the local force balance equation [24] $\partial_\nu p_{\mu\nu} + n\partial_\mu v_{\rm ext} = 0$, which can be obtained from the equation of motion. Here the first term is the internal force exerted on electrons, while the second is the external force, with $v_{\rm ext}$ being the external potential due to the nuclei. $p_{\mu\nu}$ is the stress tensor consisting of the kinetic and potential parts [36]. Clearly the external force or potential does not cause any shell structure. So, the bonding structure must arise from the internal force or stress tensor. In the uniform electron gas, the external force identically vanishes and electrons are fully delocalized. According to the local force balance condition, $p_{\mu\nu}$ must be a constant stress tensor. In inhomogeneous systems, if the pressure is high in some (bonding) regions, there must be some (intershell) regions in which the pressure is low. Therefore, the quantum pressure reflects the variation of the local force exerted on electrons and bonding structure.

In the presence of a magnetic field $\mathbf{B} = \boldsymbol{\nabla} \times \mathbf{A}$, the kinetic stress tensor [24] can be obtained by replacing the momentum operator with the canonical one, i.e.,

$$\begin{aligned} p^{\rm k}_{\mu\nu}(\mathbf{r}) &= (1/2)\langle[(-i\partial_\mu + A_\mu/c)\hat{\psi}]^\dagger[(-i\partial_\nu + A_\nu/c)\hat{\psi}] \\ &+ h.c. - \delta_{\mu\nu}\nabla^2\hat{n}/2\rangle, \end{aligned} \quad (1)$$

where c is the speed of light, $\hat{\psi}$ is the field operator, and $\hat{n}$ is the density operator. Here the density Laplacian ($\nabla^2\hat{n}$) arises from a transformation from the Laplacian ($\hat{\psi}^\dagger\partial^2_{\mu\nu}\psi$) to the gradient ($\partial_\mu\hat{\psi}^\dagger\partial_\nu\psi$) expression [35, 36], and thus is part of the stress tensor. After simple algebra, we obtain

$$p^{\rm k}(\mathbf{r}) = \frac{1}{3}{\rm Tr}\, p^{\rm k}_{\mu\nu} = \frac{2}{3}\tau - \frac{\nabla^2 n}{4} + \frac{2}{3c}\mathbf{A}\cdot\mathbf{j}_p + \frac{n}{3c^2}A^2, \quad (2)$$

where $\tau = (1/2)\sum_l |\nabla\psi_l|^2$ is the kinetic energy density, ψ_l are the Kohn-Sham occupied orbitals, and $\mathbf{j}_p$ is the paramagnetic current density defined by $\mathbf{j}_p = (1/2i)\sum_l(\psi_l^*\boldsymbol{\nabla}\psi_l - \psi_l\boldsymbol{\nabla}\psi_l^*)$. For a uniform magnetic field, $\mathbf{A} = \mathbf{B}\times\mathbf{r}/2$ satisfies the Coulomb gauge $\boldsymbol{\nabla}\cdot\mathbf{A} = 0$. From Eq. (2) we see that magnetic fields can affect $p^{\rm k}(\mathbf{r})$ explicitly by coupling to the current of electrons (last two terms), and implicitly via the orbitals.

The kinetic pressure contains $\nabla^2 n$, which originates from the definition of the stress tensor [22, 24]. It is divergent at a nucleus, where the exact pressure remains finite, because n is finite everywhere. This problem [37] can be fixed by eliminating it from Eq. (2) through the second-order gradient expansion of the kinetic energy density $\tau = \tau^{\rm TF} + |\nabla n|^2/(72n) + \nabla^2 n/6$, which is valid for slowly varying densities. Here $\tau^{\rm TF} = (3/10)(3\pi^2)^{2/3}n^{5/3}$ is the Thomas-Fermi kinetic energy density. Since the kinetic energy is a physical quantity, it should be magnetically gauge-invariant. Therefore, we should replace τ with the gauge-invariant kinetic energy density [30] $\tau - |j_p|^2/2n$ in the slowly-varying gradient expansion. This leads to

$$\begin{aligned} p^{\rm k} &= (2/3)\tau^{\rm TF} + |\nabla n|^2/(48n) - 5(\tau - \tau^{\rm TF})/6 \\ &+ 5|\mathbf{j}_p|^2/(12n) + 2\mathbf{A}\cdot\mathbf{j}_p/(3c) + nA^2/(3c^2). \end{aligned} \quad (3)$$

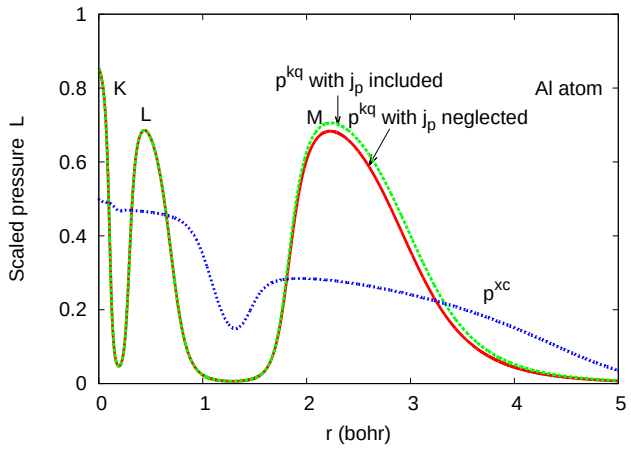

FIG. 1: Variation of the scaled pressure and its XC component for the Al atom and the effect of the paramagnetic current density. r is the radial distance from the nucleus.

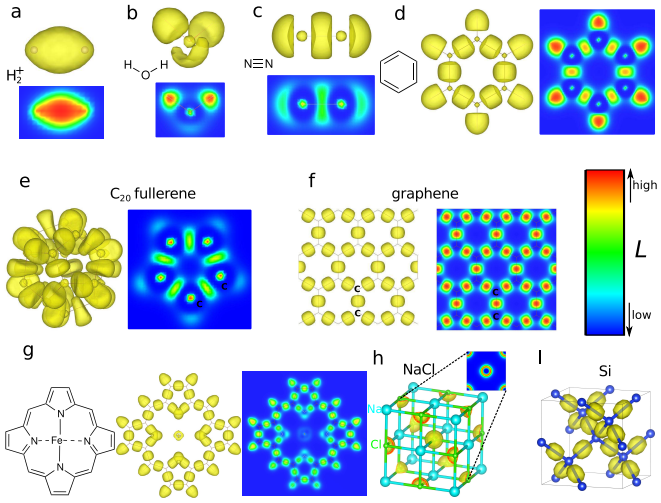

FIG. 2: Isosurfaces (gold) and image plots (blue-green-red) of the scaled quantum pressure L for (a) H_2^+, (b) H_2O, (c) N_2, (d) benzene, (e) C_{20} fullerene, (f) graphene, (g) porphyrin-Fe^{2+} complex, (h) NaCl, and (i) silicon. The isosurfaces are plotted with $L = 0.1$ for (a)-(f), $L = 0.15$ for (g), and $L = 0.5$ for (h)-(i). Except for (f)-(i) in which pseudopotentials are used, all other are performed with all-electron calculations.

(Note that $\mathbf{j}_p$ and $\mathbf{A}$ are antiparallel.) The slowly varying density is the paradigm of condensed matter physics, and the gradient expansion of the kinetic energy density has been used to eliminate the Laplacian in developing semilocal density functional approximations [18]. From Eq. (3) we see that the quantum pressure will become higher in a magnetic field, suggesting that electrons become more localized in a magnetic field [39–42]. For visualization purpose, we limit the scaled quantum pressure in the range of $0 \le L \le 1$. This can be achieved with [22]

$$L = \frac{1}{2}\left[1 + \frac{p^{\rm kq}/p^{\rm TF}}{\sqrt{1+(p^{\rm kq}/p^{\rm TF})^2}}\right], \qquad (4)$$

where $p^{\rm TF} = (2/3)\tau^{\rm TF}$ is the Thomas-Fermi classical pressure, and $p^{\rm kq}$ is the kinetic part of the quantum pressure given by

$$p^{\rm kq} = |\nabla n|^2/(48n) - 5(\tau - \tau^{\rm TF})/6 + 5|\mathbf{j}_p|^2/(12n)$$
$$+ (2/3c)\mathbf{A}\cdot\mathbf{j}_p + nA^2/(3c^2). \qquad (5)$$

To emphasize the role of the quantum effect (which vanishes in the thermodynamic limit), here we choose $p^{\rm kq}$, instead of $p^{\rm k}$, as our electron localization indicator.

Now, we turn to the potential part. Since the Hartree part does not yield atomic shell structure [22], we only consider the exchange-correlation (XC) contribution. It was shown that the XC stress tensor may be calculated with DFT-LDA [20, 21] or GGA [22] via a nonlinear coordinate transformation [21, 24]. In the presence of a magnetic field, we can calculate it from CDFT. In CDFT, a current-density functional can be written as $E_{\rm xc}[n,\mathbf{j}_p] = \int d^3r\; n\epsilon_{\rm XC}(n,\nabla n,\tau,\mathbf{j}_p)$. According to Ref. [30], current-density functionals can be constructed from ordinary density functionals. Then the XC stress tensor is obtained as $p^{\rm xc}_{ij} = \delta_{ij}[nv_{\rm xc} + \mathbf{j}_p\cdot\mathbf{A}_{\rm xc}/c] - 2\delta E_{\rm xc}/\delta g_{ij}$, where $v_{\rm xc}$ is the XC potential, and g_{ij} is the metric tensor [21, 22] for curvilinear coordinate systems. In cartesian coordinates, $g_{ij} = \delta_{ij}$. Evaluating the functional derivative of $E_{\rm xc}$ with respect to the metric tensor g_{ij} and taking the trace of the stress tensor yield the XC pressure

$$p^{\rm xc} = nv_{\rm xc} + \mathbf{j}_p\cdot\mathbf{A}_{\rm xc}/c - e_{\rm xc} - (1/3)(s\;\partial e_{\rm xc}/\partial s$$
$$+ 2\tau\;\partial e_{\rm xc}/\partial\tau + j_p\partial e_{\rm xc}/\partial j_p). \qquad (6)$$

where $j_p = |\mathbf{j}_p|$. (See SI for detailed derivation). For closed-shell systems, as in most molecules, the XC pressure is relatively small, compared to the kinetic part, because external magnetic fields only affect it through the implicit dependence of the wave function or orbitals in this case.

Figure 1 shows the scaled quantum pressure for the open-shell atom Al, the effect of the paramagnetic current density on the quantum pressure, and the XC effect, evaluated with Eqs. (4) and (6), respectively. For open-shell atoms, even when magnetic field $\mathbf{B} = 0$, there exists orbital current, due to the use of complex orbitals. In this cases, the orbital current effect can be calculated from Eq. (4), with the assumption [18] that the physical current is zero, leading to $\mathbf{A} = -c\mathbf{j}_p/n$. We can see from Fig. 1 that the atomic shell structure is largely due to the kinetic quantum pressure, while the XC effect also shows atomic shell structure similar to that exhibited by the kinetic part. The current effect is visible, though quite small.

Figure 2 shows the isosurface of the kinetic quantum pressure [Eq. (4)] and the contour plot for diverse systems

ranging from small molecules (H_2^+, H_2O, N_2, benzene), nanoscale molecules (C_{20} fullerene and porphyrin-Fe^{2+} complex), to extended systems (graphene, NaCl, and Si). In our calculations, the electron density and orbitals are generated with DFT-GGA [43], using the locally modified Octopus code [44]. The XC effect is included only implicitly via the Kohn-Sham orbitals. The top of Fig. 2(a) is the isosurface of the scaled quantum pressure for a H_2^+ molecule (paradigm in quantum chemistry), while the bottom is the contour plot. Red color represents high pressure, indicating that the electrons are localized between the nuclei to form a chemical bond.

The top of Figure 2(b) is the isosurface of a water molecule that characterizes the OH bond and the lone-pair electrons of the oxygen atom, while the contour plot at the bottom shows that the OH bond is formed by electrons localized around hydrogen atoms, due to the Coulomb repulsion from the lone electron pair on the oxygen atom. Specifically, the bright (yellow-green) area close to the oxygen nucleus represents the high pressure region arising from the two $1s$-core (K-shell) electrons. The outer blue area represents the low-pressure core-valence intershell region of the oxygen atom. The green-red area close to the hydrogen nucleus is the bonding region due to the L-shell electrons of the oxygen atom and the K-shell electron of the hydrogen atom. The light green area below the oxygen nucleus corresponds to the lone-pair electrons. Figure 2(c) illustrates the spatial variation of the quantum pressure for a N_2 molecule. From Figure 2(c) we observe that the quantum pressure is highest in the middle between two nitrogen nuclei, decays in the intershell region, and then reaches local maxima in the $1s$ core regions. We also see the signatures of core-valence intershell regions and non-bonding or lone electron pairs by the left as well as right sides of the two nitrogen atoms.

Figure 2(d)-(f) display the quantum pressure for systems with conjugated π-electrons (benzene, C_{20} fullerene, and graphene.) The variation of the quantum pressure share similar features in these three systems: all C-C bonds exhibit identical patterns with the quantum pressure, which reaches the highest value at bond midpoint and the lowest in the core-valence intershell regions. The absence of high pressure region close to carbon nuclei in C_{20} fullerene and graphene is simply due to the use of pseudopotential for carbon atoms. Figure 2(g) shows the quantum pressure of porphyrin-Fe^{2+} complex, which is of biological interest. From the image plot of Figure 2(g) we can see a small high pressure region between Fe and N atoms, indicating the chemical bonding between these two atoms, and high pressure regions between C and N atoms and between C atoms, suggesting strong bonding between these atoms. Finally we study the quantum pressure in NaCl and silicon solids. Figure 2(h) shows the isosurface of the quantum pressure in NaCl and the contour plot. From the isosurface of the quantum pressure, we see that the electrons in NaCl are basically localized around the chlorine atom, reflecting the ionic character of the Na-Cl bond, while the contour plot displays the shell structure of NaCl. Since the pseudopotential is used in solid-state calculations, the 1s core region in which the pressure is highest is not shown in the contour plot. Fig. 2(i) shows the isosurface of the quantum pressure in bulk silicon. From Fig. 2(i) we can see that electrons in silicon are largely localized in the middle region between two Si nuclei, illustrating the typical covalency of the Si-Si bond.

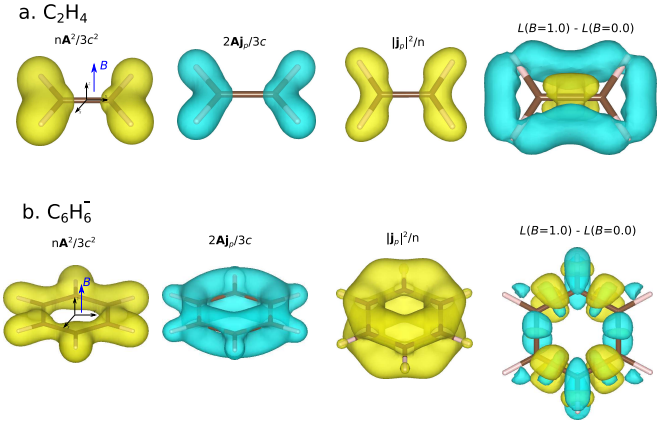

FIG. 3: The change of the quantum pressure, $\Delta L = L(B = 1) - L(B = 0)$, in (a) C_2H_4 and (b) $C_6H_6^-$, due to the external magnetic field of $B = 1$ a.u. along the z direction, and contributions from the three current-dependent terms in Eq. (3) from left to right in each panel. 1 a.u. $= 2.35 \times 10^5$ T.

Figure 3 shows the change of the kinetic quantum pressure, $\Delta L = L(B = 1) - L(B = 0)$, in (a) ethene (closed-shell) and (b) benzene anion (open-shell), in a uniform magnetic field with $B = 1.0$ a.u., and the contributions from the three current-dependent terms in Eq. (3). It can be seen from Fig. 3(a) that when we apply a magnetic field normal to the molecular plane, the quantum pressure increases around the bond axis, while it decreases in the usual π-electron region off the bond axis, suggesting that the electrons become more localized toward the bond axis. A similar phenomenon can be observed in benzene anion exposed to a magnetic field normal to the $C_6H_6^-$ plane. From Fig. 3(b), we see that, in a uniform magnetic field, the quantum pressure becomes slightly higher in the middle region of the c-c bond, suggesting that the electrons become more localized toward the bonding region between carbon atoms.

However, due to the asymmetric orbital occupation of electrons, the change in the quantum pressure is also not perfectly symmetric. Our calculations show that the magnetic field effect on the quantum pressure in $C_6H_6^-$ is much stronger than in C_2H_4 by two order of magnitudes. This is because in $C_6H_6^-$, electrons can have a circular motion generating a ring current, under the influence of the magnetic field. Finally, we calculate the difference

between the ELF of Becke and Edgecombe [12] with and without a magnetic field, ELF($B = 1$) − ELF($B = 0$), in $C_6H_6^-$. We find that the ELF can also capture the magnetic field effect, showing that, in a magnetic field, electrons become more localized between C atoms, but this effect is expectedly smaller than that on the quantum pressure.

In summary, we have formulated the quantum pressure in a magnetic field. Like an energy density, it has physical significance, although it is not uniquely defined. A nice feature of the quantum pressure is that it does not require any transformation [2]. We have demonstrated that the quantum pressure can reveal the bonding structure. This provides an alternative view on the chemical bond. Our study shows that electrons become more localized between nuclei, when a molecule is exposed to a magnetic field, but this effect can be only observable when molecules are exposed to ultrahigh magnetic fields such as those in astrophysics [40–42]. In laboratory-accessible magnetic fields, this effect is too small to be observable, as discovered experimentally in chemical reactions [33]. Since it is a local stress related to the Hamiltonian, we can study many other phenomena (e.g., spin-flip transition [45]) by incorporating various interactions such as spin-orbit coupling [46] into the quantum pressure.

We thank John P. Perdew, Youngkuk Kim, and Fenggong Wang for helpful discussions. JT acknowledges support from NSF under Grant no. CHE-1261918 and the Office of Naval Research under grant No. N00014-14-1-0761. SL acknowledges support from NSF under Grant no. CBET-1159736. FZ acknowledges support from NSF under Grant no. DMR-1124696. AMR was supported by the Department of Energy Office of Basic Energy Sciences, under Grant no. DE-FG02-07ER15920. Computational support was provided by the HPCMO and the NERSC.

* Electronic address: jianmint@sas.upenn.edu

[1] G.N. Lewis, J. Am. Chem. Soc. **38**, 762 (1916).
[2] S. Shaik, New J. Chem. **31**, 2015 (2007).
[3] C.A. Coulson, *Valence* (Clarendon Press, Oxford, 1952).
[4] L. Pauling, *The Nature of the Chemical Bond* (Cambridge University Press, London, 1960).
[5] R.G. Parr and W. Yang, *Density Functional Theory of Atoms and Molecules* (Oxford University, London, 1989).
[6] R.J. Gillespie, *Molecular Geometry* (Van Nostrand Reinhold, London, 1972).
[7] R.F.W. Bader, R.J. Gillespie, and P.J. McDougall, J. Am. Chem. Soc. 110, 7329 (1988).
[8] R. Hoffmann, J. Chem. Phys. **39**, 1397 (1963).
[9] R. Dronskowski and P.E. Blöchl, J. Phys. Chem **97**, 8617 (1993).
[10] R.F.W. Bader, *Atoms in Molecules: A Quantum Theory* (Oxford University Press, NY, 1994).
[11] A. Otero-de-la-Roza and V. Luana, J. Chem. Theory Comput. **6**, 3761 (2010).
[12] A.D. Becke and K.E. Edgecombe, J. Chem. Phys. **92**, 5397 (1990).
[13] B. Silvi and A. Savin, Nature **371**, 683 (1994).
[14] E. Matito, B. Silvi, M. Duran, and M. Solà, J. Chem. Phys. **125**, 024301 (2006).
[15] A. Savin, R. Nesper, S. Wengert, and T.F. Fssler, Angew. Chem. Int. Ed. Engl. **36**, 1808 (1997).
[16] J.K. Burdett and T.A. McCormick, J. Phys. Chem. A **102**, 6366 (1998).
[17] T. Burnus, M.A.L. Marques, and E.K.U. Gross, Phys. Rev. A **71**, 010501(R) (2005).
[18] J. Tao, J.P. Perdew, V.N. Staroverov, and G.E. Scuseria, Phys. Rev. Lett. **91**, 146401 (2003).
[19] P. de Silva and C. Corminboeuf, J. Chem. Theory Comput. 10, 3745 (2014).
[20] O.H. Nielsen and R.M. Martin, Phys. Rev. B **32**, 3780 (1985).
[21] C.L. Rogers and A.M. Rappe, Phys. Rev. B **65**, 224117 (2002).
[22] J. Tao, G. Vignale, and I.V. Tokatly, Phys. Rev. Lett. **100**, 206405 (2008).
[23] P.C. Martin and J. Schwinger, Phys. Rev. **115**, 1342 (1959).
[24] I.V. Tokatly, Phys. Rev. B **71**, 165105 (2005).
[25] J.S.M. Anderson, P.W. Ayers, and J.I.R. Hernandez, J. Phys. Chem. A **114**, 8884 (2010).
[26] K. Ichikawa *et al.,* Theor. Chem. Acc. **130**, 237 (2011).
[27] K. Finzel and M. Kohout, Theor. Chem. Acc. **132**, 1392 (2013).
[28] K. Finzel, Int. J. Quantum Chem. **114**, 568 (2014).
[29] G. Vignale and M. Rasolt, Phys. Rev. Lett. **59**, 2360 (1987).
[30] J. Tao and J.P. Perdew, Phys. Rev. Lett. **95**, 196403 (2005).
[31] A.L. Buchachenko, D.A. Kouznetsov, N.N. Bresavskaya, and M.A. Orlova, J. Am. Chem. Soc. **130**, 12868 (2008).
[32] M.T. Colvin *et al.,* J. Am. Chem. Soc. **132**, 1240 (2010).
[33] P.J. Hore, PNAS **109**, 1357 (2012).
[34] L.J. Bartolotti and R.G. Parr, J. Chem. Phys. **72**, 1593 (1980).
[35] K.-F. Berggren *et al.,* Phys. Rev. E **77**, 066209 (2008).
[36] D.N. Zubarev, *Noequilibrium Statistical Thermodynamics* (Consultants Bureau, New York, 1974).
[37] The role of $\nabla^2 n$ on the ability of the local pressure p to display the shell structure of atoms has been examined in detail in Ref. [27], both for p itself and for its Thomas-Fermi scaled counterpart (p/τ^{TF}).
[38] M. Brack, B.K. Jennings, and Y.H. Chu, Phys. Lett. **65B**, 1 (1976).
[39] B.N. Murdin *et al.,* Nature Comm. **4**, 1469 (2013).
[40] P. Schmelcher, Science **337**, 302 (2012).
[41] K.K. Lange, E.I. Tellgren, M.R. Hoffmann, and T. Helgaker, Science **337**, 327 (2012).
[42] E.I. Tellgren *et al.,* J. Chem. Phys. **140**, 034101 (2014).
[43] J.P. Perdew, K. Burke, and M. Ernzerhof, Phys. Rev. Lett. **77**, 3865 (1996).
[44] X. Andrade *et al.,* J. Phys.: Cond. Matt. **24**, 233202 (2012).
[45] J. Ibañez-Azpiroz, A. Eiguren, E.Y. Sheman, and A. Bergara, Phys. Rev. Lett. **109**, 156401 (2012).
[46] S. Liu *et al.,* J. Phys. Chem. A **118**, 9310 (2014).